Nanoscale

Dynamic Article Links

Cite this: *Nanoscale*, 2012, **4**, 2117

www.rsc.org/nanoscale

PAPER

A cerium oxide nanoparticle-based device for the detection of chronic inflammation *via* optical and magnetic resonance imaging†

Charalambos Kaittanis,[a] Santimukul Santra,[a] Atul Asati[a] and J. Manuel Perez*[ab]

Received 9th December 2011, Accepted 2nd January 2012
DOI: 10.1039/c2nr11956k

Monitoring of microenvironmental parameters is critical in healthcare and disease management. Harnessing the antioxidant activity of nanoceria and the imaging capabilities of iron oxide nanoparticles in a device setup, we were able to image changes in the device's aqueous milieu. The device was able to convey and process changes in the microenvironment's pH and reactive oxygen species' concentration, distinguishing physiological from abnormal levels. As a result under physiological and transient inflammatory conditions, the device's fluorescence and magnetic resonance signals, emanating from multimodal iron oxide nanoparticles, were similar. However, under chronic inflammatory conditions that are usually associated with high local concentrations of reactive oxygen species and pH decrease, the device's output was considerably different. Specifically, the device's fluorescence emission significantly decreased, while the magnetic resonance signal $T2$ increased. Further studies identified that the changes in the device's output are attributed to inactivation of the sensing component's nanoceria that prevents it from successfully scavenging the generated free radicals. Interestingly, the buildup of free radical excess led to polymerization of the iron oxide nanoparticle's coating, with concomitant formation of micron size aggregates. Our studies indicate that a nanoceria-based device can be utilized for the monitoring of pro-inflammatory biomarkers, having important applications in the management of numerous ailments while eliminating nanoparticle toxicity issues.

1. Introduction

The unique properties of nanomaterials have dramatically expanded the field of nanotechnology, spanning a wide spectrum of applications and industry sectors. Recent efforts have been geared towards the creation of advanced composites and devices, consisting of discrete nanoparticle building blocks.[1–5] The primary aim of this endeavour is the incorporation of the intrinsic capabilities of these building blocks into a single nanoparticle-based multifunctional system. Apart from enhanced functionality, the new apparatus can demonstrate improved performance characteristics than those of its precursor nanocomponents, such as environmental stability, stress resistance, malleability and structural integrity.[6–9] For instance, devices that encase nanoparticle formulations can protect the nanoparticles' properties, preserve the nanoparticles from non-specific agglomeration and prevent their direct interaction with cells and organs. Therefore, such a strategy is ideal for the use of powerful nanomaterials that may be classified as environmental pollutants or toxic. Particularly, nanoparticle toxicity is a major problem, because of nanomaterials' reactivity, size, composition and biological interactions. Furthermore, biological systems have evolved to utilize readily available elements, like carbon, oxygen, hydrogen, nitrogen, calcium and iron. Less abundant elements are utilized as co-factors in enzymatic complexes or can be found in chelated forms surrounded by aromatic rings and coordinated bonding. However, many elements used for nanoparticle fabrication, including rare earths, are not present in living organisms, due to their highly reactive nature that causes toxicity.[10–13] Hence, the cells do not have protective systems against these elements, whereas organisms do not have mechanisms to handle their storage, utilization and release from the body. For instance, lead and arsenic accumulate in the body and can lead to severe pathological conditions, including organ failure and death. Likewise, nanoparticles composed of metals, such as cadmium in quantum dots, are toxic.[14,15]

Despite being potent ROS scavengers and selective cytoprotective agents, recent reports demonstrate that the uptake of cerium oxide nanoparticles' (nanoceria—Ce_xO_y NP) and their intracellular residency induce dephosphorylation of various substrates, causing aberrant cell signaling and alterations in the transcriptional and post-translational levels.[16–18] Furthermore, we reported the oxidase-like activity of these nanoparticles in acidic microenvironments, which may facilitate the oxidation of intracellular and extracellular components.[19,20] Accordingly, it

[a]*Nanoscience Technology Center, University of Central Florida, Orlando, FL, USA*
[b]*Department of Chemistry, University of Central Florida, 12424 Research Pkwy, Ste 400, Orlando, FL 32826, USA. E-mail: jmperez@ucf.edu; Fax: +1 407-882-2819; Tel: +1 407-882-2843*

† Electronic supplementary information (ESI) available: ESI figures. See DOI: 10.1039/c2nr11956k

was recently demonstrated that localization of nanoceria in the acidified lysosomes induces cell death.[16] Most importantly, as cerium is not found in the human body and there are no clearance mechanisms for it, cerium may cause systemic toxicity, contrary to iron oxide nanoparticles, where their iron-containing core can be metabolized and uptaken by ferritin and transferrin. Since these findings may hinder the potential *in vivo* applications of nanoceria, encapsulation of these nanoparticles in a device might be an attractive alternative, preventing any adverse side effects from having free nanoparticles in circulation.

Considering nanoceria's potent antioxidant activities and the fact that a wide range of ailments has an associated inflammatory component accompanied with oxidative stress,[21–24] we reasoned that nanoceria might be used in a sensing-and-treatment device that monitors the overproduction of hydrogen peroxide. Hydrogen peroxide is a key player of the inflammatory response and participates in the destruction of pathogens primarily *via* the oxidative burst cascade. However, several reports implicated hydrogen peroxide, as well as other forms of reactive oxygen species (ROS), in the manifestation of various ailments, including cardiovascular diseases, rheumatoid arthritis, obesity and cancer.[25–27] Therefore, these studies highlight the importance of the *in vivo* inflammatory response monitoring *via* the assessment of the levels of these pro-inflammatory markers.[28–31] To address this clinical need, researchers have developed fluorescent probes and magnetic nanoparticles for the imaging of ROS *in vitro* and *in vivo*. These systems rely on oxidation-mediated quenching of the fluorophore,[28] ROS-induced fluorophore activation,[32] a peroxide-triggered chemiluminescence mechanism,[29] or the peroxidase-induced clustering of dopamine-carrying iron oxide nanoparticles.[33] However, a limitation of these systems is that although they report the presence of ROS, they cannot differentiate between physiological and inflammation levels of ROS, hindering clinical decision making. Thus developing a nanoceria-based multimodal system that can report the presence of aberrant levels of hydrogen peroxide might be beneficial in healthcare, particularly for vulnerable populations including the elderly and immune-suppressed patients.

Multimodal polymer-coated iron oxide nanoparticles can be ideal candidates for a hydrogen peroxide imaging system. Superparamagnetic iron oxide nanoparticles have been used as a magnetic resonance imaging (MRI) contrast agent for the imaging of cancer and metastatic lesions.[34] In an effort to introduce multimodality to these nanoparticles, researchers have encapsulated organic fluorophores and drugs within the hydrophobic pockets of the nanoparticles' coating, obtaining nanoparticles suitable for the *in vivo* assessment of the nanoparticles' localization and drugs' homing *via* magnetic resonance and fluorescence imaging.[35] Additionally, in the form of magnetic relaxation nanosensors, iron oxide nanoparticles can serve as sensitive probes for the detection of diverse biological targets and events, including cancer cells, bacteria, viruses, proteins, as well as enzymatic and metabolic activity in complex matrices, such as blood.[36] Furthermore, the target-induced aggregation of iron oxide nanoparticles has been utilized for the detection of circulating cancer and cardiac biomarkers in a multi-reservoir device, hinting the potential use of magnetic relaxation nanosensors in implantable devices.[37–39] Towards this direction, we hypothesized that nanoceria can act as the sensing component of a device that monitors the levels of H_2O_2, while the device's multimodal iron oxide nanoparticles may provide near-infrared (NIR) and magnetic resonance imaging (Fig. 1). It was anticipated that nanoceria would have been able to efficiently sequester ROS proximal to the iron oxide nanoparticles, protecting their fluorescence and MRI contrast at low and physiological concentrations of H_2O_2 (Fig. 1). However, at levels of this pro-inflammatory marker associated with chronic inflammation, the device would have yielded different outputs, due to the nanoceria's inability to scavenge the excess H_2O_2 (Fig. 1). Under these conditions, the fluorescence of the device would have decreased as a result of the oxidation-mediated fluorophore quenching, and the MRI signal would have impaired, likely due to the ROS-triggered iron oxide nanoparticle aggregation.

In this report, we utilized the antioxidant activity of nanoceria as a sensor for high levels of H_2O_2 associated with chronic inflammatory conditions, and visualized these environmental alterations using multimodal iron oxide nanoparticles. Specifically, we co-encased polyacrylic-acid-coated cerium oxide nanoparticles and NIR-emitting DiR-encapsulating dextran-coated iron oxide nanoparticles in a fabricated device. We found that in the absence of nanoceria even physiological extracellular concentrations of hydrogen peroxide could cause loss of fluorescence emission at 800 nm. On the other hand, introducing nanoceria into the device abrogated hydrogen peroxide's quenching effect, up to H_2O_2 concentrations associated with mild, transient inflammation. Interestingly, in conditions simulating chronic inflammation where the levels of hydrogen peroxide are high and frequently the extracellular milieu's pH drops, nanoceria was not able to protect the fluorophore from oxidation-induced quenching, resulting in marked decreases in the device's fluorescence emission. Apart from changes in

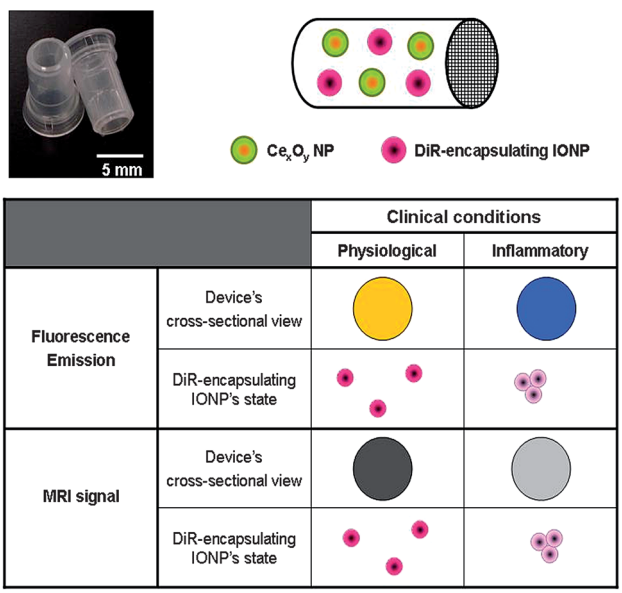

Fig. 1 Photograph of the cerium oxide nanoparticle-based device and conceptual diagram of its performance under different clinical conditions. Under physiological conditions, fluorescence emission is high, whereas the MRI signal (*T*2) is low. However under inflammatory conditions, fluorescence emission decreases, while the MRI signal (*T*2) increases.

fluorescence emission, the magnetic resonance signal was affected, with the spin–spin relaxation times ($T2$) increasing due to the prevalence of H_2O_2. We attributed these changes in the relaxation times to the extensive micron-size aggregation of iron oxide nanoparticles, due to the H_2O_2-induced polymerization of the nanoparticles' dextran coating. Particularly, the polymerization relies on the conversion of hydrogen peroxide to a hydroxyl radical and hydroxyl anion, where the iron oxide nanoparticle's Fe(II) serves as the oxidized component and Fe(III) participates in the H_2O_2 disproportionation reaction. Furthermore, utilizing the recently reported pH-dependent antioxidant activity of nanoceria, we observed that there were gradual changes in both fluorescence emission and magnetic relaxation signal as the pH of the H_2O_2-containing matrix became more acidic. Since this might have clinical implications in disease management, we visualized environmental changes with the device and clinical imaging equipment, including an MRI. Indeed, conditions that simulate chronic inflammation were created by high concentrations of H_2O_2 and low pH and induced decreases in fluorescence emission and increase in the MRI signal. Alternatively in conditions that simulate transient inflammation, both fluorescence emission and $T2$ retained their original signal. These studies demonstrate that cerium oxide nanoparticles in a device can sense inflammatory markers, while the iron oxide nanoparticles can serve as beacons that report the occurrence of inflammation-related phenomena. Also, clinically relevant imaging of hydrogen peroxide associated with severe chronic inflammation, and not with mild inflammation, is achieved *via* a multimodal nanoparticle-utilizing apparatus.

2. Experimental methods

All chemicals were obtained from Sigma and used without further processing. Hydrogen peroxide was obtained from Acros, dextran (10 kDa) from Pharmacosmos, and DiI and DiR from Invitrogen. The dextran-coated iron oxide and polyacrylic-acid-coated cerium oxide nanoparticles were prepared as previously reported.[20,40] Encapsulation of the fluorophore within the pockets of the iron oxide nanoparticles' dextran coating was achieved through the solvent diffusion method, in accordance with procedures reported in the literature.[35] After dye entrapment, the nanoparticles were dialyzed, using a 6000–8000 MWCO dialysis membrane (spectrum). The fluorophore-encapsulating iron oxide nanoparticles were stable at 4 °C in aqueous buffers (pH 6–7) over several months without any release of the dye. The device apparatus consisted of a thermopolymer dialysis chamber (10 mm length, 4 mm diameter), equipped with a 3000 MWCO cellulose membrane and was procured from Fisher. In optimization studies, we determined the optimum concentration of iron oxide nanoparticles, whereas the cerium oxide nanoparticle concentration was derived from our previous reports ([Ce_xO_y NP] = 5 μM).[20] All studies were performed at room temperature unless otherwise stated, and the averages of three independent experiments are reported. Fluorescence emission measurements were performed on an Infinite M200 multimodal reader (Tecan) and a NanoLog 3 fluorescence spectrometer (Horiba Jobin Yvon), whereas the device was imaged with either a Xenogen IVIS system or the Carestream MS FX Pro imaging station. Magnetic relaxation measurements were conducted with a compact magnetic relaxometer (0.47 T mq20, Bruker), by taking samples from the device's chamber at the end of the experiment (24 h after H_2O_2 addition). Magnetic resonance imaging of the device was achieved with a 4.7 T/200 MHz MRI spectrometer (Bruker) and an in-house-built small animal coil (AMRIS, University of Florida). Dynamic light scattering (DLS) studies were performed by placing 10 μL of the device's nanoparticle content in 990 μL of distilled water, and size changes were recorded with a PDDLS CoolBatch 40T instrument using the Precision Deconvolve 32 software. For DLS determination of dextran's polymerization, an aqueous suspension of dextran (10 mg mL^{-1}) was incubated overnight at room temperature with $FeCl_2$ and $FeCl_3$ ([Fe] = 0.01 mg mL^{-1}) and H_2O_2 ([H_2O_2] = 1 μM). X-Ray photoelectron spectroscopy was performed as we previously reported, using a Physical Electronics 5400 ESCA at the Advanced Materials Processing and Analysis Center (UCF).

3. Results and discussion

Since the nanoparticle-based device utilized dextran-coated iron oxide nanoparticles as an MRI contrast agent, we first identified organic fluorophores that demonstrated H_2O_2-mediated oxidation-induced fluorescence susceptibility. Considering their wide *in vitro* use and high quantum yield, we selected fluorophores from the indocyanine family of dyes. Hence in initial studies, we determined that the fluorophore DiR (1,1′-dioctadecyl-3,3,3′,3′-tetramethylindotricarbocyanine iodide, Invitrogen) is susceptible to H_2O_2 (1 μM) after 24 h incubation (Fig. 2A). This concentration of hydrogen peroxide was selected, since the extracellular concentrations of hydrogen peroxide involved in transient inflammatory response or signaling range from 1 to 3 μM.[41,42] Further kinetic studies revealed that the fluorophore's fluorescence emission rapidly decreased in the presence of the oxidizing agent, losing 25% of its fluorescence within ~5 h, whereas in the absence of H_2O_2 its fluorescence emission was stable (Fig. 2B).

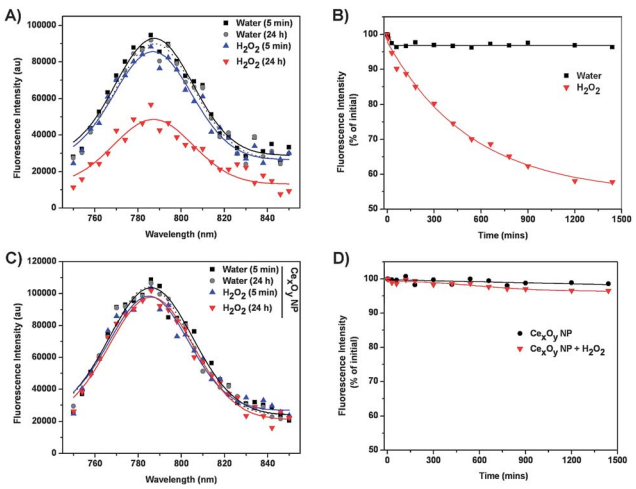

Fig. 2 Behavior of the indocyanine fluorophore DiR in the presence of H_2O_2. (A) Decrease in DiR's fluorescence emission after 24 h incubation with H_2O_2 (1 μM). (B) Hydrogen peroxide mediates the gradual loss of the fluorophore's fluorescence over time. (C) Cerium oxide nanoparticles (Ce_xO_y NP) preserve DiR's fluorescence emission from hydrogen peroxide. (D) The dye retains its fluorescence in the presence of H_2O_2, upon treatment with nanoceria (Ce_xO_y NP).

These results suggested that indocyanine fluorophores, such as DiR and DiI (1,1′-dioctadecyl-3,3,3′3′-tetramethylindocarbocyanine perchlorate), can be sensitive fluorescent probes for hydrogen peroxide. Interestingly, at physiological pH (pH 7) and in the presence of nanoceria ($D = 5$ nm), DiR's fluorescence was marginally affected by hydrogen peroxide even after 24 h (Fig. 2C and D), similar to its analogue DiI (Fig. S1A and S1B, ESI†). This can be attributed to nanoceria's ability to scavenge ROS, preventing the dye's oxidation-triggered fluorescence decrease. Additional spectroscopic studies revealed that both DiR and DiI are photostable at physiological and acidic pH, since pH did not induce any changes in the fluorescence emission profile (Fig. S2A and S2B, and S3A and S3B, ESI†, respectively). Taken together, these data suggest that indocyanine fluorophores, like DiR and DiI, are robust at clinically relevant pH levels, potentially facilitating the detection of abnormal levels of H_2O_2.

Having established that nanoceria protects cyanine-related dyes in solution from hydrogen peroxide, we reasoned that cerium oxide nanoparticles can similarly prevent DiR-encapsulating dextran-coated iron oxide nanoparticles ($D = 77$ nm, $r^2 = 195$ mM^{-1} s^{-1}) from any H_2O_2-induced quenching in a device setting. Having a length of 10 mm and a diameter of 4 mm, the device allowed the diffusion of small molecules but blocked the escape of nanoparticles, due to the presence of a 3000 MWCO cellulose membrane (Fig. 1).

Our results indicated that the fluorescence emission of DiR-encapsulating iron oxide nanoparticles was unaffected at pH 7 in the presence of nanoceria and H_2O_2 (1 μM) (Fig. 3A). However, hydrogen peroxide induced more than 25% reduction in the device's fluorescence emission, when nanoceria was not part of the device (Fig. 3A). Subsequently, we wanted to establish if the nanoceria-containing device was sensitive enough, capable of distinguishing mild *vs.* chronic inflammatory H_2O_2 concentrations. We found that under transient and mild inflammatory conditions, simulated by extracellular H_2O_2 concentrations between 1 and 3 μM,[41,42] the device's fluorescence was comparable to that obtained in the absence of H_2O_2 (Fig. 3A and B).

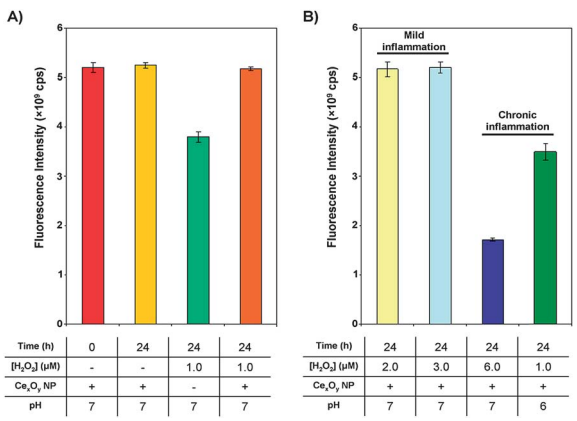

Fig. 3 Fluorescence emission of the device at different pathological states. (A) Ce_xO_y NP preserves the near-infrared fluorescence of DiR-encapsulating iron oxide nanoparticles from H_2O_2 levels associated with mild, transient inflammatory conditions. (B) Under chronic inflammation, the device's fluorescence emission significantly decreases.

Plausibly at these hydrogen peroxide levels, the device's nanoceria was able to scavenge the generated reactive oxygen species, *via* cerium oxide's nanoparticle regenerative antioxidant activity. On the other hand, 6 μM H_2O_2 resulted in a marked decrease in fluorescence emission, indicating that nanoceria could not protect the fluorophore from oxidation-induced inactivation, likely due to the rapid buildup of high levels of reactive oxygen species (Fig. 3B). Likewise, as chronic inflammation and cancer are associated with a drop in the extracellular milieu's pH, we found that nanoceria at pH 6 could not deter the H_2O_2-mediated quenching of the iron oxide nanoparticle's fluorescence (Fig. 3B). This was expected as previous reports have demonstrated that the acidification of the nanoceria's aqueous milieu gradually inactivates its antioxidant property.[19,20] To further corroborate that the mechanism of the fluorophore's deprotection is attributed to inactivation of nanoceria's antioxidant activity, at either low pH or high H_2O_2 levels, we utilized X-ray photoelectron spectroscopy. Indeed similar to previous reports, our results indicated that under these abnormal conditions the content of Ce^{4+} was higher than that of Ce^{3+} (ESI, Table S1†). This is typical of a non-regenerative nanoceria system that is unable to sequester ROS, including H_2O_2.[20] Overall these results demonstrate that the fluorescent device can detect high levels of hydrogen peroxide and chronic inflammation related to low pH (acidosis) and ROS generation, based on nanoceria's environmentally controlled antioxidant activity.

In subsequent studies, we investigated whether hydrogen peroxide affects the device's magnetic resonance signal ($T2$), similar to what happens to its fluorescence emission. Utilizing a bench-top magnetic relaxometer (0.47 T Minispec, Bruker) and a NIR-recording animal imaging station (IVIS, Xenogen), we found that H_2O_2 (1 μM) in the absence of nanoceria was able to not only change the device's fluorescence signal, but also alter the device's magnetic resonance signature (Table 1). Specifically, hydrogen peroxide induced increases in the $T2$ relaxation times, which were prevented when nanoceria was incorporated in the device (Table 1). These results were surprising, since to the best of our knowledge, no reports have previously demonstrated that hydrogen peroxide can affect the relaxation times of an aqueous solution containing iron oxide nanoparticles. Therefore to further elucidate this phenomenon, we employed dynamic light scattering (DLS) analysis, in order to determine the nanoparticles' state. Interestingly, we found that the DiR-encapsulating iron oxide nanoparticles had an initial average diameter of 77 nm and were well dispersed in solution (Fig. 4A and the inset). However, in the presence of 1 μM H_2O_2 but in the absence of nanoceria, the emergence of a second population was observed (>1 μm), consisting of large aggregates (Fig. 4B and the inset).

Table 1 Ce_xO_y NP retains the device's fluorescence and spin–spin relaxation ($T2$) signals from ROS ([H_2O_2] = 1 μM)

	MR signal/ms			Fluorescence intensity/×10⁹ cps	
	$T2_{Initial}$	$T2_{24\ h}$	$\Delta T2$	Initial	24 h
No Ce_xO_y NP	165 ± 3	280 ± 5	115	5.2 ± 0.1	3.8 ± 0.1
With Ce_xO_y NP	163 ± 2	166 ± 4	3	5.2 ± 0.1	5.3 ± 0.1

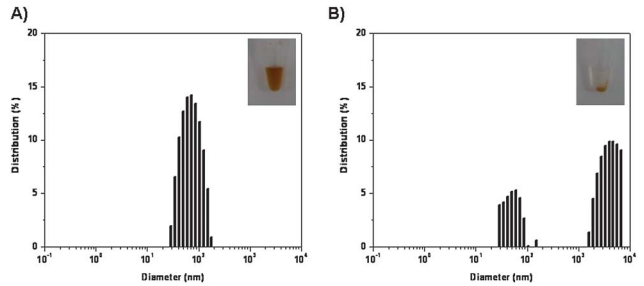

Fig. 4 Size distribution of DiR-encapsulating iron oxide nanoparticles prior (A) and after addition of H_2O_2 (1 μM) (B). (Insets: photographs of concentrated iron oxide nanoparticle preparations in the absence or presence of hydrogen peroxide, indicating that this oxidizing agent causes nanoparticle precipitation.)

Thus in accordance with our hypothesis, these results demonstrated that hydrogen peroxide can effectively induce the aggregation of the device's iron oxide nanoparticles in the absence of nanoceria, consequently causing increases in the magnetic relaxation signal. Similarly under chronic inflammatory conditions where nanoceria is unable to sequester the excess ROS, hydrogen peroxide can cause nanoparticle aggregation, with concomitant changes in the $T2$ signal. The H_2O_2-mediated nanoparticle micron-size aggregation differs from the target-induced nanoparticle clustering, which results in the formation of supramolecular assemblies below 1 μm with concomitant $T2$ decreases, due to the entrapment of water molecules within the intricate nanoparticle network.[43] In order to further delineate the mechanism of the iron oxide nanoparticles' aggregation, we investigated whether hydrogen peroxide was affecting their dextran coating. Since iron oxide nanoparticles possess peroxidase activity,[44] we reasoned that the nanoparticles' iron (Fe^{2+}/Fe^{3+}) may participate in a Fenton reaction, yielding radicals that can promote the cross-linking and polymerization of the nanoparticle dextran coating. We employed dynamic light scattering analysis, because it has been reported that dextrans of different molecular weights adopt a particular coil conformation in solution with distinct dimensions and sizes. For instance, a 500 kDa dextran has a diameter of 29.4 nm (Stokes radius = 14.7 nm), whereas a 10 kDa dextran, similar to that coating the device's iron oxide nanoparticles, is roughly 4.8 nm (Stokes radius ≈ 2.4 nm)[45] (Fig. 5A). Therefore through DLS, we identified that H_2O_2 mediated dextran's polymerization (Fig. 5B), which was enhanced and more effective in the presence of Fe^{2+}/Fe^{3+} ions (Fig. 5C). Plausibly, the device's iron oxide nanoparticle aggregation can be mechanistically ascribed to the H_2O_2-mediated polymerization of the dextran coating, imminently reflected in the nanoparticle's size and device's $T2$ signal.

Acknowledging that nanoceria exhibits pH-dependent antioxidant activity, we investigated whether the device's fluorescence and magnetic resonance signals can sense H_2O_2 during changes in the environment's pH. Such a capability is ideal, because the extracellular matrix's pH is tightly regulated by a complex homeostatic cascade, whereas decreases in the pH are associated with disease. For instance, cancer manifestation and metastasis are accompanied by a drop in the interstitial pH, due to cancer cells' metabolic divergence from oxidative phosphorylation to glycolysis in a process described as the Warburg effect.[46] Therefore, we incubated the device in the presence of H_2O_2 (1 μM) and buffers adjusted to normal and slightly acidic pH, resembling physiological and cancerous conditions. As expected, results indicated that the device's outputs were affected by H_2O_2 in a pH-regulated process. Specifically, the $T2$ magnetic relaxation signal increased as the pH dropped (Fig. 6A, $r = -0.994$), indicating that gradual inactivation of nanoceria's free-radical-scavenging activity led to aggregation of the iron oxide nanoparticles. Similarly, when the aqueous milieu's pH incrementally acidified, the device's fluorescence slowly decreased in a linear trend (Fig. 6B, $r = 0.989$). Hence this can be justified by the oxidation-triggered quenching of DiR, upon pH-dependent inactivation of nanoceria's antioxidant capacity, suggesting that the device can sense microenvironmental alterations associated with disease.

Finally, we examined whether changes in the device's fluorescence and magnetic resonance signal can be imaged using a lab-based fluorescence imaging station (MS FX PRO, Carestream) and a 33 cm bore MRI (4.7 T, Bruker). Results indicated that the device's fluorescence emission and magnetic resonance signal were retained under transiently inflammatory conditions (1 μM H_2O_2, pH 7), having comparable values to those of the control device that was placed under physiological conditions (0 μM H_2O_2, pH 7) (Fig. 7). However, in the presence of 6 μM H_2O_2 (pH 7), the device's fluorescence emission decreased, while the $T2$ signal increased. This indicates that the device responded to such acute levels of the proinflammatory marker. Additionally, since chronic inflammation is accompanied with acidosis in disease states, like primary tumor formation and metastasis, we examined how the device responds at acidosis-relevant pH (pH 6) and elevated levels of hydrogen peroxide. As deemed by its reduced fluorescence emission and high $T2$ signal (Fig. 7), the

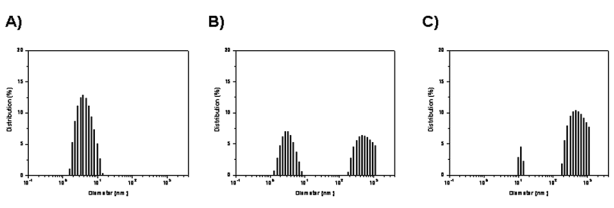

Fig. 5 Size distribution of 10 kDa dextran in the absence (A) and presence of hydrogen peroxide (1 μM) (B). (C) Extensive aggregation of the polymer in the presence of hydrogen peroxide and iron ions (Fe^{2+}/Fe^{3+}).

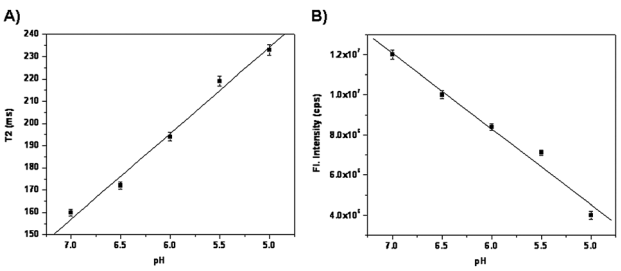

Fig. 6 The pH-dependent loss of Ce_xO_y NP's antioxidant activity results in the gradual de-protection of the device's magnetic resonance (A) and fluorescence signals (B) due to H_2O_2 (1 μM).

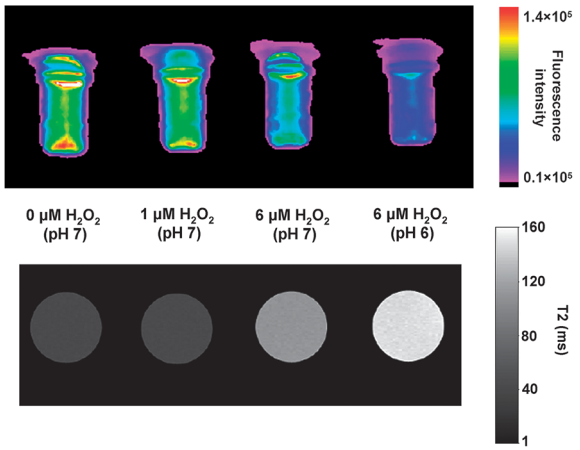

Fig. 7 The device reports the presence of aberrant levels of inflammation through the changes in fluorescence emission and MRI signal (*T2*). Images depict the device's coronal plane during fluorescence-based imagining and its transverse plane during MRI.

device could assess these non-physiological conditions through *in vivo* capable multimodal instrumentations.

4. Conclusions

In conclusion, we have demonstrated that a nanoceria-based device can detect abnormal levels of hydrogen peroxide and microenvironmental alterations through changes in the device's fluorescence and magnetic resonance signals. Specifically, the device's cerium oxide nanoparticles act as the hydrogen peroxide sensor, being able to differentiate between transient inflammatory levels (1–3 μM H_2O_2) and chronic inflammatory concentrations (>3 μM H_2O_2). Considering that nanoceria can sequester other forms of ROS, such as superoxide and nitroxyl radicals,[17,47] the device can potentially sense a plethora of inflammatory mediators, other than hydrogen peroxide. Additionally, irregular changes in the pH related to the inflammatory response can prevent nanoceria from preserving the signal output of the reporting iron oxide nanoparticles, leading to distinct signal profiles. For medical applications, this system can be utilized as a standalone implantable device or prosthetic equipment's component. For instance, it can have applications in a broad range of ailments with a proinflammatory component, including inflammatory bowel disease, ulcerative colitis, cystic fibrosis, sepsis, cardiovascular disease, arthritis, multiple sclerosis and Alzheimer's disease.[21–27] Furthermore, as acidosis and ROS interfere with cancer chemotherapy,[23] the device can be utilized as an implant in cancer therapeutic regimes. Additionally, patients with transplants or prosthetic apparatuses may utilize the nanoceria-based device for the *in vivo* monitoring of the post-operative inflammatory response, as the device can be further miniaturized and integrated to the prosthetic organ. This inflammation-monitoring system may overall monitor aberrant inflammatory conditions *via* irreversible changes to its nanoscale components that result in alterations in the device's output signal, allowing the physician to cumulatively assess the microenvironmental milieu and proceed on necessary therapeutic interventions. Moreover, as the iron oxide nanoparticles' polymeric coating can accommodate a plethora of fluorophores, the device may provide multispectral imaging capabilities, for the monitoring of environmental and industrial samples. Overall, considering its sensitivity, robustness and imaging capabilities, the use of this nanoceria-based device in medicine, industry and environmental protection should be anticipated.

Acknowledgements

This work was supported by the National Institute of General Medical Sciences GM084331 grant to JMP and an American Foundation for Aging Research graduate fellowship to CK. The authors thank Dr Glenn Walter (AMRIS, UF) for his technical assistance with the MR imaging and the AMPAC personnel (UCF) for the XPS analyses.

Notes and references

1 S. Behrens, *Nanoscale*, 2011, **3**, 877–892.
2 T. Dvir, B. P. Timko, D. S. Kohane and R. Langer, *Nat. Nanotechnol.*, 2011, **6**, 13–22.
3 C. Minelli, S. B. Lowe and M. M. Stevens, *Small*, 2010, **6**, 2336–2357.
4 J. Lee, S. Mahendra and P. J. Alvarez, *ACS Nano*, 2010, **4**, 3580–3590.
5 O. Akbulut, A. A. Yu and F. Stellacci, *Chem. Soc. Rev.*, 2010, **39**, 30–37.
6 A. S. Iyer and L. A. Lyon, *Angew. Chem., Int. Ed.*, 2009, **48**, 4562–4566.
7 S. Nayak and L. A. Lyon, *Angew. Chem., Int. Ed.*, 2005, **44**, 7686–7708.
8 D. Peer, J. M. Karp, S. Hong, O. C. Farokhzad, R. Margalit and R. Langer, *Nat. Nanotechnol.*, 2007, **2**, 751–760.
9 A. K. Boal, F. Ilhan, J. E. DeRouchey, T. Thurn-Albrecht, T. P. Russell and V. M. Rotello, *Nature*, 2000, **404**, 746–748.
10 C. Carlson, S. M. Hussain, A. M. Schrand, L. K. Braydich-Stolle, K. L. Hess, R. L. Jones and J. J. Schlager, *J. Phys. Chem. B*, 2008, **112**, 13608–13619.
11 B. C. Schanen, A. S. Karakoti, S. Seal, D. R. Drake, 3rd, W. L. Warren and W. T. Self, *ACS Nano*, 2009, **3**, 2523–2532.
12 S. M. Hussain and J. J. Schlager, *Toxicol. Sci.*, 2009, **108**, 223–224.
13 A. Nel, T. Xia, L. Madler and N. Li, *Science*, 2006, **311**, 622–627.
14 N. Chen, Y. He, Y. Su, X. Li, Q. Huang, H. Wang, X. Zhang, R. Tai and C. Fan, *Biomaterials*, 2012, **33**, 1238–1244.
15 B. A. Rzigalinski and J. S. Strobl, *Toxicol. Appl. Pharmacol.*, 2009, **238**, 280–288.
16 A. Asati, S. Santra, C. Kaittanis and J. M. Perez, *ACS Nano*, 2010, **4**, 5321–5331.
17 J. M. Perez, A. Asati, S. Nath and C. Kaittanis, *Small*, 2008, **4**, 552–556.
18 M. H. Kuchma, C. B. Komanski, J. Colon, A. Teblum, A. E. Masunov, B. Alvarado, S. Babu, S. Seal, J. Summy and C. H. Baker, *Nanomed.: Nanotechnol., Biol. Med.*, 2010, **6**, 738–744.
19 A. Asati, C. Kaittanis, S. Santra and J. M. Perez, *Anal. Chem.*, 2011, **83**, 2547–2553.
20 A. Asati, S. Santra, C. Kaittanis, S. Nath and J. M. Perez, *Angew. Chem., Int. Ed.*, 2009, **48**, 2308–2312.
21 E. C. Hadley, E. G. Lakatta, M. Morrison-Bogorad, H. R. Warner and R. J. Hodes, *Cell*, 2005, **120**, 557–567.
22 D. A. Butterfield, J. Drake, C. Pocernich and A. Castegna, *Trends Mol. Med.*, 2001, **7**, 548–554.
23 H. Y. Chung, M. Cesari, S. Anton, E. Marzetti, S. Giovannini, A. Y. Seo, C. Carter, B. P. Yu and C. Leeuwenburgh, *Ageing Res. Rev.*, 2009, **8**, 18–30.
24 E. Shacter, J. A. Williams, R. M. Hinson, S. Senturker and Y. J. Lee, *Blood*, 2000, **96**, 307–313.
25 W. Zhao, *Angew. Chem., Int. Ed.*, 2009, **48**, 3022–3024.
26 C. Tortorella, G. Piazzolla and S. Antonaci, *Immunopharmacol. Immunotoxicol.*, 2001, **23**, 565–572.
27 J. Vitte, B. F. Michel, P. Bongrand and J. L. Gastaut, *J. Clin. Immunol.*, 2004, **24**, 683–692.
28 A. Tsourkas, G. Newton, J. M. Perez, J. P. Basilion and R. Weissleder, *Anal. Chem.*, 2005, **77**, 2862–2867.

29 D. Lee, S. Khaja, J. C. Velasquez-Castano, M. Dasari, C. Sun, J. Petros, W. R. Taylor and N. Murthy, *Nat. Mater.*, 2007, **6**, 765–769.
30 E. W. Miller, A. E. Albers, A. Pralle, E. Y. Isacoff and C. J. Chang, *J. Am. Chem. Soc.*, 2005, **127**, 16652–16659.
31 W. T. Chen, C. H. Tung and R. Weissleder, *Mol. Imaging*, 2004, **3**, 159–162.
32 P. Panizzi, M. Nahrendorf, M. Wildgruber, P. Waterman, J. L. Figueiredo, E. Aikawa, J. McCarthy, R. Weissleder and S. A. Hilderbrand, *J. Am. Chem. Soc.*, 2009, **131**, 15739–15744.
33 J. M. Perez, F. J. Simeone, A. Tsourkas, L. Josephson and R. Weissleder, *Nano Lett.*, 2004, **4**, 119–122.
34 M. G. Harisinghani, J. Barentsz, P. F. Hahn, W. M. Deserno, S. Tabatabaei, C. H. van de Kaa, J. de la Rosette and R. Weissleder, *N. Engl. J. Med.*, 2003, **348**, 2491–2499.
35 S. Santra, C. Kaittanis, J. Grimm and J. M. Perez, *Small*, 2009, **5**, 1862–1868.
36 C. Kaittanis, S. Santra and J. M. Perez, *Adv. Drug Delivery Rev.*, 2010, **62**, 408–423.
37 K. D. Daniel, G. Y. Kim, C. C. Vassiliou, F. Jalali-Yazdi, R. Langer and M. J. Cima, *Lab Chip*, 2007, **7**, 1288–1293.
38 K. D. Daniel, G. Y. Kim, C. C. Vassiliou, M. Galindo, A. R. Guimaraes, R. Weissleder, A. Charest, R. Langer and M. J. Cima, *Biosens. Bioelectron.*, 2009, **24**, 3252–3257.
39 Y. Ling, T. Pong, C. C. Vassiliou, P. L. Huang and M. J. Cima, *Nat. Biotechnol.*, 2011, **29**, 273–277.
40 C. Kaittanis, S. Nath and J. M. Perez, *PLoS One*, 2008, **3**, e3253.
41 X. Liu and J. L. Zweier, *Free Radical Biol. Med.*, 2001, **31**, 894–901.
42 S. T. Test and S. J. Weiss, *J. Biol. Chem.*, 1984, **259**, 399–405.
43 C. Kaittanis, S. Santra, O. J. Santiesteban, T. J. Henderson and J. M. Perez, *J. Am. Chem. Soc.*, 2011, **133**, 3668–3676.
44 L. Gao, J. Zhuang, L. Nie, J. Zhang, Y. Zhang, N. Gu, T. Wang, J. Feng, D. Yang, S. Perrett and X. Yan, *Nat. Nanotechnol.*, 2007, **2**, 577–583.
45 J. K. Jaiswal, S. Chakrabarti, N. W. Andrews and S. M. Simon, *PLoS Biol.*, 2004, **2**, E233.
46 M. G. Vander Heiden, L. C. Cantley and C. B. Thompson, *Science*, 2009, **324**, 1029–1033.
47 C. Korsvik, S. Patil, S. Seal and W. T. Self, *Chem. Commun.*, 2007, 1056–1058.